**SCIENCE CHINA**
Information Sciences

• **Supplementary File** •

# Randomized Multimodel Multiple Hypothesis Tracking

Haiqi LIU[1], Xiaojing SHEN[1*], Zhiguo WANG[1] & Fanqin MENG[2]

[1]*School of Mathematics, Sichuan University, Chengdu, Sichuan* 610064*, China;*
[2]*School of Automation and Information Engineering, Sichuan University of Science and Engineering, Yibin* 644000*, China*

## Appendix A The calculation of Likelihood ratios

A global hypothesis is composed of compatible track hypotheses, where tracks are said to be compatible if they have no measurements in common. Specifically, a global hypothesis $\gamma$ is defined as

$$\gamma = \{(\tau^i, \mathbf{s}^i, \mathbf{r}^i)\}_{i=0}^{n(\gamma)}, \tag{A1}$$

$$\mathbf{r}^{i_1} \cap \mathbf{r}^{i_2} = \emptyset \text{ or } 0, \text{ for } i_1 \neq i_2, \tag{A2}$$

$$\cup_{i=0}^{n(\gamma)} \tau^i = \{\tau\}_{\tau=0}^{T}, \tag{A3}$$

$$\cup_{i=0}^{n(\gamma)} \mathbf{r}^i = \cup_{n=1}^{N} \{r_n\}_{r_n=1}^{R_n}. \tag{A4}$$

Note that when $\tau^i = 0$, $(0, \mathbf{s}^i, \mathbf{r}^i)$ means that the measurements with indices $\mathbf{r}^i$ are hypothesized as false alarms. Let $\Gamma^*$ be the finite collection of all global hypotheses $\gamma$, and $\Gamma$ be a random element defined on $\Gamma^*$. The likelihood ratio of the global hypothesis is defined as

$$\frac{P(\Gamma = \gamma | \mathbf{Z}^N)}{P(\Gamma = \gamma^0 | \mathbf{Z}^N)}, \tag{A5}$$

where $\gamma$ is a global hypothesis satisfied (A1)-(A4), and $\gamma_0$ is a reference global hypothesis, i.e., all measurements are false alarms.

Let $\Omega^N$ denote the event that a global hypothesis $\gamma$ is true, and $\Omega_0^N$ denote the event that $\gamma^0$ is true, the likelihood ratio (A5) becomes

$$\frac{P(\Omega^N | \mathbf{Z}^N)}{P(\Omega_0^N | \mathbf{Z}^N)}. \tag{A6}$$

Moreover, we assume that $\Omega^N = \psi^N \cup \Omega^{N-1}$, where $\Omega^{N-1}$ is a specific global hypothesis up to the previous scan that produce $\Omega^N$, $\psi^N$ is the association hypothesis at the $(k+N)$-th scan. The numerator in (A6) can be expanded as follows using Bayes' rule,

$$P(\Omega^N | \mathbf{Z}^N) = \frac{p(\mathbf{Z}_{k+N} | \Omega^N, \mathbf{Z}^{N-1}) P(\psi^N | \Omega^{N-1}, \mathbf{Z}^{N-1})}{p(\mathbf{Z}_{k+N} | \mathbf{Z}^{N-1})} P(\Omega^{N-1} | \mathbf{Z}^{N-1}), \tag{A7}$$

The terms in the numerator are expanded as follows,

$$p(\mathbf{Z}_{k+N} | \Omega^N, \mathbf{Z}^{N-1}) = \prod_{r_N \in R_N^d} p_t(\mathbf{z}_{k+N}^{r_N} | \mathbf{Z}^{N-1}, \Omega^N) \prod_{r_N \in R_N^f} p_f(\mathbf{z}_{k+N}^{r_N}), \tag{A8}$$

$$P(\psi^N | \Omega^{N-1}, \mathbf{Z}^{N-1}) = \frac{\exp(-\lambda_f) \lambda_f^{R_N}}{R_N!} (1 - P_d)^{T - d_N} \left( \frac{P_d}{\lambda_f} \right)^{d_N}, \tag{A9}$$

where $R_N^d$ and $R_N^f$ in (A8) are the sets of indices of detections and false alarms on scan $k+N$, respectively, $T$ is the number of targets, and $d_N$ is the number of detections on scan $k+N$. Note that $R_N^d \cup R_N^f = \{r_N\}_{r_N=1}^{R_N}$ and $R_N^d \cap R_N^f = \emptyset$. More details and intuitive interpretations can be seen in [1].

Normalizing by dividing by $P(\Omega_0^N | \mathbf{Z}^N)$ yields

$$\begin{aligned} \frac{P(\Omega^N | \mathbf{Z}^N)}{P(\Omega_0^N | \mathbf{Z}^N)} &= \frac{P(\Omega^{N-1} | \mathbf{Z}^{N-1})}{P(\Omega_0^{N-1} | \mathbf{Z}^{N-1})} \cdot \{(1 - P_d)^{T - d_N} \prod_{r_N \in R_N^d} [\frac{P_d p_t(\mathbf{z}_{k+N}^{r_N} | \mathbf{Z}^{N-1}, \Omega^N)}{\lambda_f p_f(\mathbf{z}_{k+N}^{r_N})}]\} \\ &= \prod_{n=1}^{N} \{(1 - P_d)^{T - d_n} \prod_{r_n \in R_n^d} [\frac{P_d p_t(\mathbf{z}_{k+n}^{r_n} | \mathbf{Z}^{n-1}, \Omega^N)}{\lambda_f p_f(\mathbf{z}_{k+n}^{r_n})}]\}. \end{aligned} \tag{A10}$$

* Corresponding author (email: shenxj@scu.edu.cn)

Based on (A10), we define the likelihood ratio of a local hypothesis $(\tau, \mathbf{s}, \mathbf{r})$ as follows,

$$L_{(\tau,\mathbf{s},\mathbf{r})} = \prod_{n=1}^{N} (1-P_d)^{1-\delta_{r_n}^n} \left[ \frac{P_d p_t(\mathbf{z}_{k+n}^{r_n} | \mathbf{Z}^{n-1}, \Omega^N)}{\lambda_f p_f(\mathbf{z}_{k+n}^{r_n})} \right]^{\delta_{r_n}^n}, \tag{A11}$$

where $\delta_{r_n}^n$ is binary variable with $\delta_{r_n}^n = 1$ if $r_n \neq 0$, and $\delta_{r_n}^n = 0$ otherwise. Moreover, since each local hypothesis $(\tau, \mathbf{s}, \mathbf{r}) \in \Omega^N$ is assumed independent from the other local hypotheses in $\Omega^N$ [2], (A10) can be represented by the product of the likelihood ratio $L_{(\tau,\mathbf{s},\mathbf{r})}$, i.e.,

$$\frac{P(\Omega^N | \mathbf{Z}^N)}{P(\Omega_0^N | \mathbf{Z}^N)} = \prod_{(\tau,\mathbf{s},\mathbf{r}) \in \Omega^N} L_{(\tau,\mathbf{s},\mathbf{r})}. \tag{A12}$$

Note that since the measurement noise is assumed Gaussian, the likelihood function of $\mathbf{z}_{k+n}^{r_n}$ given $\mathbf{Z}^{n-1}$ and $\Omega^N$ is

$$p_t(\mathbf{z}_{k+n}^{r_n} | \mathbf{Z}^{n-1}, \Omega^N) = \mathcal{N}(\mathbf{z}_{k+n}^{r_n}; \hat{\mathbf{z}}_{k+n}^{\tau}, \mathbf{S}_{k+n}^{\tau}),$$

where $r_n \in (\tau, \mathbf{s}, \mathbf{r})$, $(\tau, \mathbf{s}, \mathbf{r}) \in \Omega^N$, $\hat{\mathbf{z}}_{k+n}^{\tau}$ and $\mathbf{S}_{k+n}^{\tau}$ are the predicted measurement and the corresponding covariance calculated by a Kalman filter based on $\hat{\mathbf{x}}_{k|k}^{\tau}$ and $\mathbf{P}_{k|k}^{\tau}$ of target $\tau$ and model $s_{n-1}$, respectively. Specifically, given a track hypothesis $(\tau, \mathbf{s}, \mathbf{r})$ and the measurements $\mathbf{Z}^N$, we calculate $\hat{\mathbf{x}}_{k+n-1|k+n-1}^{\tau}$ and $\mathbf{P}_{k+n-1|k+n-1}^{\tau}$ using the Kalman filter based on the measurements $\{\mathbf{z}_{k+1}^{r_1}, \cdots, \mathbf{z}_{k+n-1}^{r_{k+n-1}}\}$ and the model indices $(s_1, \cdots, s_{n-1})$. Then, the predicted state and covariance can be obtained by

$$\begin{aligned}
\hat{\mathbf{x}}_{k+n|k+n-1}^{\tau} &= F_{k+n-1}^{(s_n)} \hat{\mathbf{x}}_{k+n-1|k+n-1}^{\tau}, \\
\mathbf{P}_{k+n|k+n-1}^{\tau} &= F_{k+n-1}^{(s_n)} \mathbf{P}_{k+n-1|k+n-1}^{\tau} (F_{k+n-1}^{(s_n)})' + \mathbf{Q}^{(s_n)},
\end{aligned}$$

where $\mathbf{Q}^{(s_n)}$ is the covariance of process noise $v_{k+n-1}^{(s_n)}$. The predicted measurement and innovation covariance are calculated by

$$\begin{aligned}
\hat{\mathbf{z}}_{k+n}^{\tau} &= H_{k+n} \hat{\mathbf{x}}_{k+n|k+n-1}^{\tau}, \\
\mathbf{S}_{k+n}^{\tau} &= H_{k+n} \mathbf{P}_{k+n|k+n-1}^{\tau} H_{k+n}' + \mathbf{R}_{k+n}^{r_n},
\end{aligned}$$

where $\mathbf{R}_{k+n}^{r_n}$ is the covariance of measurement noise $w_{k+n}^{r_n}$.

## Appendix B State estimation via RCMKF

Based on (8), the random coefficient matrix measurement equation for the measurement vector $\mathbf{z}_{k+1}$ is

$$\mathbf{z}_{k+1} = \mathbf{h}_{k+1} \mathbf{X}_{k+1} + \mathbf{w}_{k+1}, \tag{B1}$$

where $\mathbf{h}_{k+1} = ((\mathbf{h}_{k+1}^1)', \cdots, (\mathbf{h}_{k+1}^{R_1})')'$, $\mathbf{w}_{k+1} = ((\mathbf{w}_{k+1}^1)', \cdots, (\mathbf{w}_{k+1}^{R_1})')'$, and $\mathrm{Cov}(\mathbf{w}_{k+1}) = \mathbf{R}_{k+1}$. Similarly, based on (10), the random coefficient matrix state equation for the joint state vector $\mathbf{X}_k$ is defined as

$$\mathbf{X}_{k+1} = \mathbf{F}_k \mathbf{X}_k + \mathbf{v}_k, \tag{B2}$$

where $\mathbf{F}_k = \mathrm{diag}(\mathbf{F}_k^1, \cdots, \mathbf{F}_k^T)$, $\mathbf{v}_k = ((\mathbf{v}_k^1)', \cdots, (\mathbf{v}_k^T)')'$, and $\mathrm{Cov}(\mathbf{v}_k) = \mathbf{Q}_k$.

We denote $\widetilde{\mathbf{F}}_k = \mathbf{F}_k - \overline{\mathbf{F}}$ and $\tilde{\mathbf{h}}_{k+1} = \mathbf{h}_{k+1} - \bar{\mathbf{h}}$, where $\overline{\mathbf{F}} = E(\mathbf{F}_k)$ and $\bar{\mathbf{h}} = E(\mathbf{h}_{k+1})$. Then, (B2) and (B1) are rewritten as

$$\mathbf{X}_{k+1} = \overline{\mathbf{F}} \mathbf{X}_k + \tilde{\mathbf{v}}_k, \tag{B3}$$

$$\mathbf{z}_{k+1} = \bar{\mathbf{h}} \mathbf{X}_{k+1} + \tilde{\mathbf{w}}_{k+1}, \tag{B4}$$

where $\tilde{\mathbf{v}}_k = \mathbf{v}_k + \widetilde{\mathbf{F}}_k \mathbf{X}_k$, and $\tilde{\mathbf{w}}_{k+1} = \mathbf{w}_{k+1} + \tilde{\mathbf{h}}_{k+1} \mathbf{X}_{k+1}$. Then, the state estimation is obtained by RCMKF:

$$\mathbf{X}_{k+1|k+1} = \mathbf{X}_{k+1|k} + \mathbf{K}_{k+1}(\mathbf{z}_{k+1} - \bar{\mathbf{h}} \mathbf{X}_{k+1|k}), \tag{B5}$$

$$\mathbf{P}_{k+1|k+1} = (\mathbf{I} - \mathbf{K}_{k+1} \bar{\mathbf{h}}) \mathbf{P}_{k+1|k}, \tag{B6}$$

$$\mathbf{X}_{k+1|k} = \overline{\mathbf{F}} \mathbf{X}_{k|k}, \tag{B7}$$

$$\widetilde{\mathbf{Q}}_k = \mathbf{Q}_k + E(\widetilde{\mathbf{F}}_k E(\mathbf{X}_k \mathbf{X}_k') \widetilde{\mathbf{F}}_k'), \tag{B8}$$

$$\mathbf{P}_{k+1|k} = \overline{\mathbf{F}} \mathbf{P}_{k|k} \overline{\mathbf{F}}' + \widetilde{\mathbf{Q}}_k, \tag{B9}$$

$$E(\mathbf{X}_{k+1} \mathbf{X}_{k+1}') = \overline{\mathbf{F}} E(\mathbf{X}_k \mathbf{X}_k') \overline{\mathbf{F}}' + E(\widetilde{\mathbf{F}}_k E(\mathbf{X}_k \mathbf{X}_k') \widetilde{\mathbf{F}}_k') + \mathbf{Q}_k, \tag{B10}$$

$$\widetilde{\mathbf{R}}_{k+1} = \mathbf{R}_{k+1} + E(\tilde{\mathbf{h}} E(\mathbf{X}_{k+1} \mathbf{X}_{k+1}') \tilde{\mathbf{h}}'), \tag{B11}$$

$$\mathbf{K}_{k+1} = \mathbf{P}_{k+1|k} \bar{\mathbf{h}}' (\bar{\mathbf{h}} \mathbf{P}_{k+1|k} \bar{\mathbf{h}}' + \widetilde{\mathbf{R}}_{k+1})^{\dagger}, \tag{B12}$$

where $(\cdot)^{\dagger}$ is the Moore-Penrose inverse. Note that the most computationally intensive part of the RCMKF is the matrix inverse in (B12). Let $R_1$ denote the number of valid measurements, then the computational complexity of the RCMKF is $\mathcal{O}(R_1 \cdot m)^3$, where $m$ is the dimension of the measurement.

## Appendix C Track management

### Track initialization

There are a number of methods to initialize a new track, such as the single-point method [3], and the two-point method [4]. The key to track initialization is how to select the points to form a track. In the framework of RMM-MHT, we consider to use the unassigned measurements to initialize tracks. However, the measurements are associated with targets in a probabilistic sense, and the unassigned measurements cannot be provided directly. Thus, we use the unassigned probability $P^h_{0,r_n}$ to evaluate whether a measurement is unassigned, where $P^h_{0,r_n}$ is defined as

$$P^h_{0,r_n} := \sum_{\mathbf{s}} \sum_{(r_1,\cdots,r_{n-1},r_{n+1},\cdots,r_N)} P_{(0,\mathbf{s},\mathbf{r})}.$$

Given a large threshold $P^{\text{unas}}_{\text{th}}$, if $P^h_{0,r_n} > P^{\text{unas}}_{\text{th}}$, then measurement $r_n$ is unassigned and can be used in track initialization. For $n = 1,\cdots,N$, we collect the unassigned measurements of each scan, and denote the unassigned measurements as $\mathbf{Z}^u = ((\mathbf{z}^u_{k+1})',\cdots,(\mathbf{z}^u_{k+N})')'$, where $\mathbf{z}^u_{k+n} = ((\mathbf{z}^{u,1}_{k+n})',\cdots,(\mathbf{z}^{u,R^u_n}_{k+n})')'$, and $R^u_n$ is the number of unassigned measurements at time $k+n$.

Let $\mathbf{r} = (r_1,\cdots,r_N)$ denote the hypothesis of a new track, and $P_{\mathbf{r}}$ be the probability that $\mathbf{r}$ forms a new track. The track initialization problem can be formulated as follows:

$$\begin{aligned}
&\text{Minimize } \sum_{\mathbf{r}} C_{\mathbf{r}} P_{\mathbf{r}} \\
&\text{Subject to:} \\
&\qquad \sum_{\mathbf{r}\setminus\{r_n\}} P_{\mathbf{r}} = 1, \\
&\qquad \text{for } n = 1,\cdots,N \text{ and } r_n = 1,\cdots,R^u_n, \\
&\qquad 0 \leqslant P_{\mathbf{r}} \leqslant 1 \text{ for all } \mathbf{r}.
\end{aligned} \tag{C1}$$

The cost coefficient $C_{\mathbf{r}}$ can be defined based on the maximum likelihood estimation [5]. When the solution of (C1) is obtained and $P_{\mathbf{r}}$ is greater than a given threshold $P^{\text{init}}_{\text{th}}$, i.e., $P_{\mathbf{r}} > P^{\text{init}}_{\text{th}}$, we use the measurements with indices $\mathbf{r} = (r_1,\cdots,r_N)$ to initialize a track.

### Track pruning

We define a specific track $\tau$ which loses measurements at time $k+n$, if the probability $P^h_{\tau,r_n=0}$ that it loses measurements is greater than a given threshold $P^{\text{miss}}_{\text{th}}$, i.e., $P^h_{\tau,r_n=0} > P^{\text{miss}}_{\text{th}}$. Here, $P^h_{\tau,r_n=0} := \sum_{\mathbf{s}} \sum_{(r_1,\cdots,r_{n-1},r_{n+1},\cdots,r_N)} P_{(\tau,\mathbf{s},\mathbf{r}^{n,0})}$, where $\mathbf{r}^{n,0} = (r_1,\cdots,r_{n-1},0,r_{n+1},\cdots,r_N)$. Further, a track $\tau$ is pruned, if it loses measurements in $N_{\text{miss}}$ consecutive scans, where $N_{\text{miss}}$ is a given threshold for track pruning [6].

## Appendix D Randomized Multimodel MHT Algorithm

**Algorithm D1** Randomized Multimodel MHT Algorithm

**Require:** $\{\mathbf{x}^\tau_k\}^T_{\tau=1}$; $\{\mathbf{z}_{k+1},\cdots,\mathbf{z}_{k+N}\}$;
**Ensure:** $\{\mathbf{x}^\tau_{k+1}\}^T_{\tau=1}$

1: Track maintenance:
- establish the objective function (6);
- minimize (6) under the constraints (2)–(3) by the LP algorithm;
- obtain the probabilities of data associations and dynamic models, and establish the system (B2) and (B1);
- update the system (B2) and (B1) by the RCMKF (B5)–(B12) and obtain the state estimates $\{\hat{\mathbf{x}}^\tau_{k+n}\}^T_{\tau=1}$, for $n = 1,\cdots,N$.
- update confirmed tracks $\{\mathbf{x}^\tau_k\}^T_{\tau=1}$ to $\{\mathbf{x}^\tau_{k+1}\}^T_{\tau=1}$.

2: Collect unassigned measurements: $\{\mathbf{z}^u_{k+1},\cdots,\mathbf{z}^u_{k+N}\}$;
3: Track initialization:
- solve problem (C1);
- using measurements with indices $\mathbf{r}$ to initialize new tracks $\{\overline{\mathbf{x}}^m_{k+1}\}^M_{m=1}$ when $P_{\mathbf{r}} > P^{\text{init}}_{\text{th}}$.

4: Output tracks in the current scan $k+N$:
- For confirmed tracks $\{\mathbf{x}^\tau_{k+1}\}^T_{\tau=1}$, output $\{\hat{\mathbf{x}}^\tau_{k+N}\}^T_{\tau=1}$;
- For new tracks $\{\overline{\mathbf{x}}^m_{k+1}\}^M_{m=1}$, output $\{\hat{\overline{\mathbf{x}}}^m_{k+1}\}^M_{m=1}$.

5: Integrate the new tracks into the confirmed tracks: $\{\mathbf{x}^\tau_{k+1}\}^T_{\tau=1} = \{\mathbf{x}^\tau_{k+1}\}^T_{\tau=1} \bigcup \{\overline{\mathbf{x}}^m_{k+1}\}^M_{m=1}$;
6: set $k = k+1$;

## Appendix E Simulation results

In this section, we compare the performance of the proposed RMM-MHT method with that of the IMM-MHT method. To demonstrate the performance of RMM-MHT, we consider a typical MMTT scenario where we include both closely spaced targets and maneuvering targets described in [4]. The implementation of the MHT algorithm is the TOMHT, where the corresponding multidimensional assignment problem is solved by the Lagrangian relaxation algorithm [7]. The hypothesis depths of RMM-MHT and IMM-MHT are 2 scans, i.e., making association decisions using 2 scans of measurement data.

The true trajectories of the three targets are shown in Fig. E1. As shown in Fig. E1, the three targets fly westward with their motion described by the constant velocity (CV) model, before executing a $1^\circ/s$ coordinated turn based on the constant turn (CT) model. Then the three targets fly southward based on the CV model, followed by a $3^\circ/s$ coordinated turn based on the CT model. Finally, they continue to fly westward based on the CV model after the turn.

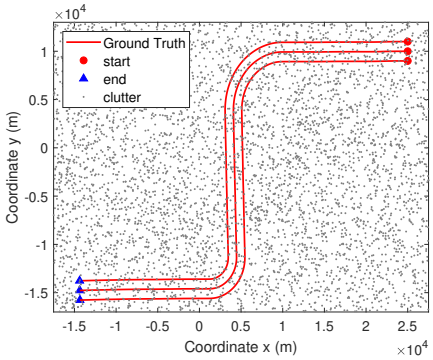


**Figure E1** Scenario: Ground truth and clutter.

The simulation parameters are set as follows: the measurement model is the target position plus Gaussian noise of zero mean and standard deviation 400m. The clutter model assumes that the clutter returns originate from points that are uniformly distributed over the surveillance region, while the number of clutter returns is assumed to follow the Poisson distribution with a known mean $\lambda_f = 50$ during each scan (see Fig. E1). The target space is set to 1000m. For each target, the one-point method [3] is applied for track initialization, and the initial distribution is known as a priori distribution.

In the simulation, we consider using two CV models with different process noises to describe a single target state transition equation. In general, the specific parameters of the turning speed are not known, but it is reasonable to use a large variance in the CV model to represent target maneuvers [4]. Specifically, the state equation for a single target $\tau$ is $\mathbf{x}_{k+1}^{\tau} = F_k \mathbf{x}_k^{\tau} + v_k^{(s_1)}$, $s_1 = 1, 2$, where

$$F_k = \begin{bmatrix} 1 & \Delta T & 0 & 0 \\ 0 & 1 & 0 & 0 \\ 0 & 0 & 1 & \Delta T \\ 0 & 0 & 0 & 1 \end{bmatrix},$$

and the covariance of the process noise $v_k^{(s_1)}$ is

$$Q = q^{(s_1)} \cdot \begin{bmatrix} \Delta T^3/3 & \Delta T^2/2 & 0 & 0 \\ \Delta T^2/2 & \Delta T & 0 & 0 \\ 0 & 0 & \Delta T^3/3 & \Delta T^2/2 \\ 0 & 0 & \Delta T^2/2 & \Delta T \end{bmatrix}. \tag{E1}$$

The parameters of the process noises of the two CV models are set to $q^{(1)} = 0.01\mathrm{m}^2/\mathrm{s}^3$ and $q^{(2)} = 4\mathrm{m}^2/\mathrm{s}^3$, respectively. As the mode transition probabilities are given in [4], we consider to use the following three mode transition probability matrices in the IMM-MHT method:

$$P^{(1)} = \begin{bmatrix} 0.95 & 0.05 \\ 0.1 & 0.9 \end{bmatrix}, \quad P^{(2)} = \begin{bmatrix} 0.95 & 0.05 \\ 0.2 & 0.8 \end{bmatrix}, \quad P^{(3)} = \begin{bmatrix} 0.95 & 0.05 \\ 0.3 & 0.7 \end{bmatrix}.$$

The corresponding IMM filters are denoted by IMM-P1, IMM-P2, and IMM-P3, respectively. And the corresponding IMM-MHT methods are denoted by IMM-MHT-P1, IMM-MHT-P2, and IMM-MHT-P3, respectively. The results of the simulation for RMM-MHT and IMM-MHT are compared using the tracking performance index: the average of the optimal sub-pattern assignment (OSPA) distance $d_p^c(X, Y)$ [8] over 100 Monte Carlo simulation runs, where the cutoff parameter $c = 3000$ and the order parameter $p = 1$. In Fig. E2(a), the OSPA distances of the IMM filter based on different mode transition probability matrices are plotted as a function of the time steps, where we assume that the data association is correct and the sampling period is $\Delta T = 5$s same as [4]. In Figs. E2(b)-E2(d), the OSPA distances of the IMM-MHT and RMM-MHT for different sampling periods with $\Delta T = 1$s, 5s, and 10s are plotted as a function of the time steps, respectively. In Figs. E3(a)-E3(c), the average probability of the three targets operating in the maneuvering mode ($q = 4\mathrm{m}^2/\mathrm{s}^3$) is plotted for different sampling periods with $\Delta T = 1$s, 5s, and 10s, respectively.

From Figs. E2(a)-E3(c), we have the following observations:

1. Fig. E2(a) shows that, for this scenario, if there are no data association problems, the overall performance of the IMM filter is not sensitive to the mode transition probability matrix, except during the maneuvering stage, which is consistent with [4, 9].

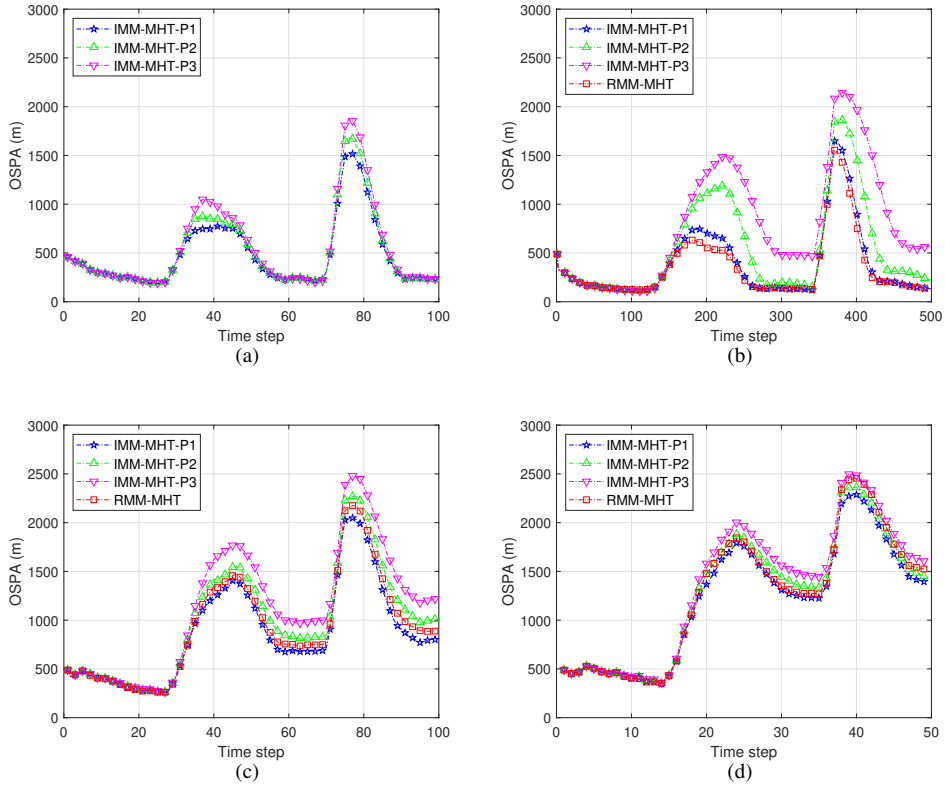


**Figure E2** OSPA results: (a) OSPA distances for different mode transition probability matrices with the sampling period $\Delta T = 5$s; (b) OSPA distances for IMM-MHT and RMM-MHT with the sampling period $\Delta T = 1$s; (c) OSPA distances for IMM-MHT and RMM-MHT with the sampling period $\Delta T = 5$s; (d) OSPA distances for IMM-MHT and RMM-MHT with the sampling period $\Delta T = 10$s.

2. Comparing Fig. E2(a) with Fig. E2(c), both of them with the sampling period $\Delta T = 5$s, Fig. E2(c) shows that when there are data association problems, the overall performance of IMM-MHT is sensitive to the mode transition probability matrix, where it has a difference during both the maneuvering stage and subsequent non-maneuvering stage. Since if the IMM filter has a worse performance during the maneuvering stage like in Fig. E2(a), it would lead to an incorrect data association so that the overall performance becomes worse.

3. Figs. E2(b)-E2(d) illustrate that when the sampling period increases, the performances of RMM-MHT and IMM-MHT under the three mode transition probability matrices become worse. The reason is that the target maneuvering index is relative to the sampling period, when the sampling period increases, the target maneuvering index becomes large [4]. Therefore, with the same model set, when the target maneuvering index increases, the performances of both methods become worse.

4. Figs. E3(a)-E3(c) show that the model switching probabilities of RMM-MHT have a similar trend as IMM-MHT for the sampling period of 1s, 5s, and 10s. It is closer to the best namely IMM-MHT-P1. Figs. E2(b)-E2(d) also show that the OSPA performance of RMM-MHT is closer to that of the best IMM-MHT-P1, even though RMM-MHT does not require and use prior mode transition probabilities. The reason is that the model probabilities of the IMM-MHT are optimized under the condition that the association relationship between targets and measurements has been fixed. However, the model switching probability of RMM-MHT is derived by jointly optimizing the multiple possible models and measurement association hypotheses.

5. For the same reason, Figs. E2(b)-E2(d) also show that RMM-MHT works close to the optimal IMM-MHT-P1 for a small target maneuvering index (i.e., small sampling period of 1s). The difference between RMM-MHT and IMM-MHT becomes small for a large target maneuvering index (i.e., large sampling period of 10s). Thus, RMM-MHT is more suitable when the target maneuvering index is small and the mode transition probability matrix is unknown. Table E1 shows the runtimes of the compared methods using a MATLAB implementation on a single core of an Intel Core i7-4700MQ CPU@2.40GHz. The runtimes are averaged over 100 simulation runs. These results confirm that the proposed RMM-MHT has a lower computational complexity.

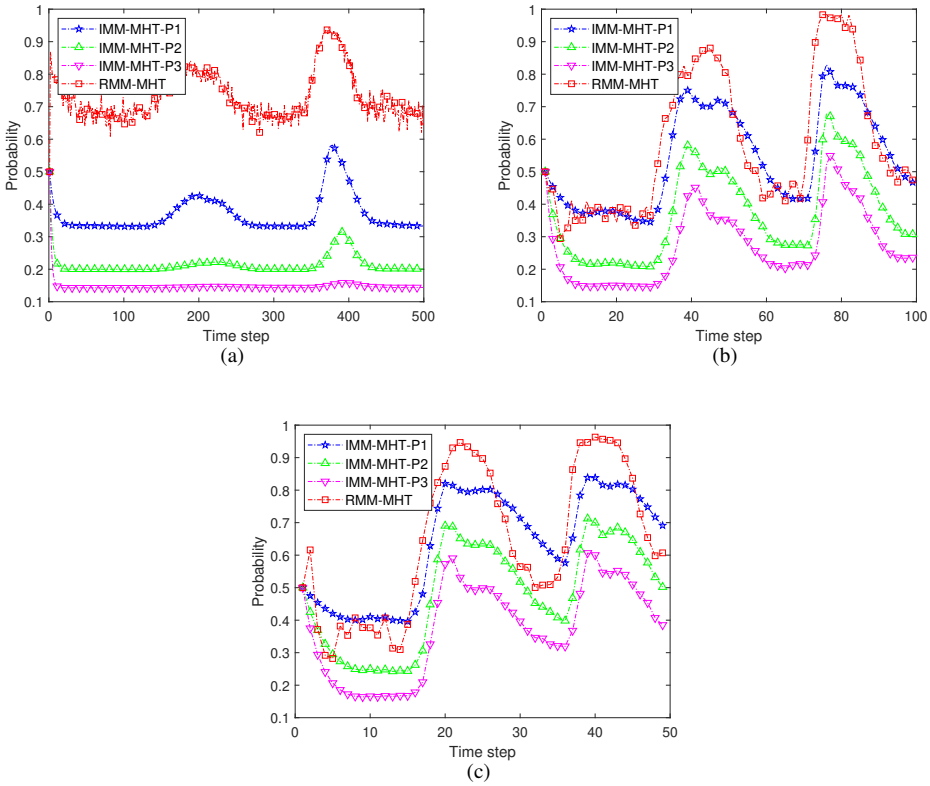


**Figure E3** Mode probabilities results: Probability of the target operating in the maneuvering mode ($q = 4\mathrm{m}^2/\mathrm{s}^3$) with the sampling period (a) $\Delta T = 1$s; (b) $\Delta T = 5$s; (c) $\Delta T = 10$s.

**Table E1** The computational time of the compared methods.

| | $\Delta T = 1$s | $\Delta T = 5$s | $\Delta T = 10$s |
|---|---|---|---|
| IMM-MHT-P1 | 60.7288s | 14.3181s | 8.2789s |
| IMM-MHT-P2 | 60.8408s | 14.0360s | 8.0569s |
| IMM-MHT-P3 | 60.3779s | 13.6632s | 7.8131s |
| RMM-MHT | 19.1838s | 4.6119s | 2.8994s |

**References**


1 Poore A B. Multidimensional assignment formulation of data association problems arising from multitarget and multisensor tracking. Comput Optim Appl, 1994, 3: 27–57.
2 Morefield C. Application of 0-1 integer programming to multitarget tracking problems. IEEE Trans Automa Control, 1977, 22: 302–312.
3 Mallick M, La Scala B. Comparison of single-point and two-point difference track initiation algorithms using position measurements. Acta Automatica Sinica, 2008, 34: 3, 258–265.
4 Bar-Shalom Y, Li X R, Kirubarajan T. Estimation with applications to tracking and navigation: theory algorithms and software. John Wiley & Sons, 2004.
5 Deb S, Yeddanapudi M, Pattipati, K, and Bar-Shalom Y, A generalized S-D assignment algorithm for multisensor-multitarget state estimation, IEEE Trans Aerosp Electron Syst, 1997, 33: 2, 523–538.
6 Mallick M, Coraluppi S, Carthel C. Multitarget tracking using multiple hypothesis tracking. In Mahendra Mallick, Vikram Krishnamurthy, and Ba-Ngu Vo, editors, Integrated Tracking, Classification, and Sensor Management, chapter 5, Wiley/IEEE, 2012, 165–201.
7 Poore A B, Robertson III A J. A new Lagrangian relaxation based algorithm for a class of multidimensional assignment problems. Comput Optim Appl, 1997, 8: 129–150.
8 Schuhmacher D, Vo B T, Vo B N. A consistent metric for performance evaluation of multi-object filters. IEEE Trans Signal Process, 2008, 56: 8, 3447–3457.

9 Li X R, Jilkov V P. Survey of maneuvering target tracking. Part V: Multiple-model methods. IEEE Trans Aerosp Electron Syst, 2005, 41: 4, 1255–1321.